Journal of The Electrochemical Society, **166** (10) A1785-A1792 (2019)
0013-4651/2019/166(10)/A1785/8/$38.00 © The Electrochemical Society

Improved Composite Solid Electrolyte through Ionic Liquid-Assisted Polymer Phase for Solid-State Lithium Ion Batteries

Jiahua Ou,[=] Gaoran Li,[=] and Zhongwei Chen *,z

Department of Chemical Engineering, Waterloo Institute for Nanotechnology, Waterloo Institute for Sustainable Energy, University of Waterloo, Waterloo, Ontario N2L 3G1, Canada

Organic-inorganic solid-state composite electrolyte is of great promise to support the high-performance and safe energy storage applications. Herein we developed an ionic liquid-assisted PEO-LAGP-EMITFSI composite electrolyte (PLE) for advanced solid-state lithium ion batteries (LIBs). The EMITFSI ionic liquid was employed as the plasticizer to effectively lower the crystallinity of the composite and thus significantly enhance the ionic conductivity up to 8.85×10^{-4} S cm^{-1} at 60°C. Combined with its good electrochemical stability and decent ion transference selectiveness, the optimized PLE electrolyte contributed to an excellent battery performance in $LiFePO_4$/PLE/Li configuration with high capacity retention of 114.7 mAh g^{-1} after 120 cycles and good rate capability of 112.2 mAh g^{-1} at 1C, indicating its great potential in developing high-performance solid-state LIBs.
 [DOI: 10.1149/2.0401910jes]

Manuscript submitted April 3, 2019; revised manuscript received May 17, 2019. Published May 31, 2019.

Lithium ion batteries (LIBs) have achieved a tremendous commercial success in the past few decades. However, as the rapid development of portable electronics, electrical vehicles, and grid-scale energy storage system, the conventional LIBs are struggling to face the ever-growing demands in terms of energy density and safety performance. The development of advanced electrolyte plays critical roles in promoting the next-generation high-performance batteries. Electrolyte is an essential ingredient in battery configuration, which undertakes the responsibility of transporting Li^+ ions for the redox reactions in both cathode and anode. Compared to its liquid counterpart in conventional LIBs, solid state electrolyte (SSE) delivers intriguing superiorities such as wide electrochemical window, high volumetric efficiency, non-leakage and non-flammability, holding a great promise in fulfilling high-energy-density and high-safety LIBs.[1–5] Whereas in addition to the cost issue, the intrinsically low ionic conductivity of SSE and the sluggish electrode/electrolyte interfacial charge transfer are still impeding the SSE from practical implementation.[6–12]

SSE can be generally classified into two categories, namely, organic and inorganic solid electrolytes. Inorganic oxide ceramic solid electrolytes such as $Li_7La_3Zr_2O_{12}$ (LLZO), $Li_{1.5}Al_{0.5}Ge_{1.5}P_3O_{12}$ (LAGP), and $Li_{6.55}La_3Zr_2Ga_{0.15}O_{12}$ (Ga-LLZO), usually deliver high ionic conductivity (10^{-4} to 10^{-3} S cm^{-1}),[4] yet their grain boundary resistance is often the bottleneck for the total conductivity.[13] The brittleness limits their practical thickness in cells, and the rigid nature of most oxide ceramics renders poor electrolyte/electrode contact which can be exacerbated during cycling due to periodic electrode volume change.[14] While inorganic sulfide glass-ceramic and glassy electrolytes such as $Li_{10}GeP_2S_{12}$ (LGPS), and $75Li_2S$-$25P_2S_5$ exhibit high ionic conductivity (10^{-3} to 10^{-2} S cm^{-1}) with low grain boundary resistance, it comes with the detriment of their instability against lithium compared to oxide counterparts, and their sensitivity to oxygen and moisture.[15] On the other hand, the organic category represented by poly(ethylene oxide) (PEO)-based electrolyte, maintains a more uniform contact against the electrode benefiting from the soft polymer chains. The soft, flexible nature of PEO also enables thin, flexible films to be fabricated in the orders of tens of micrometers which is a benefit in lowering overall cell resistance as well as pave the way for future flexible batteries. However, their bulk conductivity is poor (10^{-6} to 10^{-4} S cm^{-1}) due to the intrinsic ion hopping conduction mechanism and limits their practical use as a stand-alone electrolyte mechanism.[16,17] Given this, composite electrolyte is highly promising and has been widely investigated to combine the advantages of organic and inorganic solid electrolyte while mitigating their disadvantages.[18–23] Ceramic electrolyte powder dispersed in polymer matrix has been widely studied to take advantage of the high ionic conductivity of ceramic and the low interfacial resistance of polymer. Small additions of ceramic electrolyte into PEO such as 1 wt% of LGPS have shown to improve ionic conductivity as well as widen electrochemical stability window against lithium anode.[21] Low loadings of ceramic electrolyte can decrease the overall crystallinity of the polymer and provide additional Li^+ diffusion pathways which improves ionic conductivity and lowers activation energy.[18,24,25] In order to further improve the electrochemical performance of the composite electrolyte, higher loadings of ceramic electrolyte in PEO have been studied. Wang et al.[26] prepared LAGP-PEO composite membrane with extremely high LAGP loading (99%), which showed ionic conductivity reaching 1.1×10^{-5} S cm^{-1} at room temperature, compared to 1.5×10^{-4} S cm^{-1} for a sintered pure LAGP pellet. The 14 times setback in conductivity largely stems from the high grain boundary resistance between unsintered LAGP particles. Although some grain boundary resistance can be mitigated through PEO by providing improved physical contact compared to loose LAGP powder, energy barrier for which Li^+ has to overcome between ceramic-polymer interface can depreciate the increase of ionic conductivity as LAGP content versus polymer approaches unity. As micro-voids may also appear during the drying process,[27] a more efficient approach to improving the performance of such composite electrolyte may lie in the polymer phase instead of increasing LAGP loading which can be costly.

Herein, we developed an ionic liquid (IL)-assisted organic-inorganic composite electrolyte, namely, PEO_{16}LiTFSI-LAGP-EMITFSI (PLE), for advanced solid-state LIBs. The introduction of l-Ethyl-3-methylimidazolium bis-(trifluoromethylsulfonyl)-imide (EMITFSI) not only reduces the crystallinity of PEO in the electrolyte composite, but also improves the ionic contact at the ceramic particle/particle as well as the electrode/electrolyte interfaces, thus facilitating the ion transfer in both bulk electrolyte and the interfaces. A high conductivity of 6.20×10^{-5} S cm^{-1} can be achieved at 30°C and 8.85×10^{-4} cm^{-1} at 60°C for the optimized PLE electrolyte. Apart from that, the as-developed composite electrolyte also shows good electrochemical stability with electrochemical window of 1.5–5.5 V (vs. Li^+/Li), and a relatively high lithium transference number of 0.73. The $LiFePO_4$ electrode based on the as-developed PLE composite electrolyte shows an initial capacity of 143.5 mAh g^{-1}, and an excellent cyclability with a capacity retention of 114.7 mAh g^{-1} at 0.3C, over 120 cycles. The composite electrolyte also delivers decent rate capability with 112.2 mAh g^{-1} at high rate of 1 C. These results demonstrate the great superiority of the PLE composite electrolyte, which holds great promise in advancing the development of solid-state batteries.

Experimental

Preparation of composite electrolyte.—PEO (Mn = 400,000), Lithium bis(trifluoromethane-sulfonyl)imide (LiTFSI), and EMITFSI

[=]These authors contributed equally to this work.
*Electrochemical Society Member.
[z]E-mail: zhwchen@uwaterloo.ca

were purchased from Sigma-Aldrich Inc. LiTFSI salt was vacuumed dried at 80°C for 24 hours before storage an d use in argon-filled glove box. PEO and LiTFSI were weighed at molecular ratio of [EO]:[Li] = 16:1. LAGP was purchased from MTI Corp, with purity of 99.99%, and average particle size of 500 nm. LAGP and EMITFSI were then added as a certain weight ratio to PEO and dissolved in acetonitrile to form PEO_{16}LiTFSI-LAGP-EMITFSI (PLE) slurry. LAGP pellet was compressed in a die set and sintered in air at 800°C for 6 hours.

Cell assembly.—The cathode slurry was prepared by adding active material $LiFePO_4$ (LFP) and Super P carbon to the PLE slurry at weight ratio of 10:3:7 and dissolved in acetonitrile. The electrolyte and cathode slurries were sealed in a vial and stirred on a hotplate at 50°C for 48 and 72 hours respectively. The slurries were further mixed respectively in a high-shear mixer multiple times before casting to minimize phase separation. The cathode slurry was cast on aluminum current collector with a doctor blade, and dried under vacuum at room temperature for 24 hours. The electrolyte slurry was then directly cast on top of the cathode layer and similarly dried before transferring to an argon-filled glove box. The samples were remained in the glove box for 24 hours before the cell assembly to eliminate moisture. Lithium foil was used as anode by being pressed onto a stainless-steel (SS) current collector and attached to the electrolyte layer to construct $LiFePO_4$/PLE/Li configuration in CR2032 coin cells.

Physical characterization.—The X-ray diffraction patterns of the composite electrolytes was obtained through X-ray diffraction (XRD). Thermal properties were characterized by TA Instruments Q2000 differential scanning calorimeter (DSC) with scanning rate of 10°C min^{-1} from −80 to 95°C. One heating/cooling cycle was first performed on the samples to remove thermomechanical history before collecting data on the following heating segment. Morphology and elemental mapping were obtained through Zeiss Leo 1530 scanning electron microscope (SEM).

Electrochemical measurements.—The electrochemical window of the composite electrolytes was measured through linear sweeping voltammetry (LSV) from OCV to −0.5 and to 6.5 V at 0.1 mV s^{-1}. The cell was constructed as SS/PLE/Li in a coin cell. Ionic conductivity was measured by electrochemical impedance spectroscopy (EIS) in symmetric SS/PLE/SS coin cells within the frequency range of 1 MHz to 0.1 Hz at an amplitude of 10 mV. LAGP pellet ionic conductivity was measured similarly after coating both sides of the pellet with silver paste as blocking electrodes. To obtain the lithium transference number (t_{Li+}) of the PLE, Li/PLE/Li coin cells were fabricated. EIS was first recorded from 1MHz to 0.1 Hz at 10 mV. The cells were then polarized by applying a constant voltage of 10 mV for 5 hours, when all the cells have reached steady state. EIS was then performed again after polarization to obtain cell resistance. By applying Bruce and Vincent's work on transference number, which is suited for solid polymer electrolytes, steady state lithium transference number can be calculated through Eq. 1,[28,29]

$$t_{Li+} = \frac{I_{ss}\left(\Delta V - I_o R_{B,o}\right)}{I_o\left(\Delta V - I_{SS} R_{B,ss}\right)} \quad [1]$$

where ΔV refers to applied potential, I_o and I_{SS} are measured currents at the beginning and steady state value during polarization, respectively; $R_{B,O}$ and $R_{B,SS}$ are bulk resistances of the composite electrolytes measured through EIS before and post-polarization, respectively. Cells constructed with $LiFePO_4$, lithium foil, and PLE composite as cathode, anode, and electrolyte respectively, were tested for electrochemical performances using LAND2001A cycler. The electrolyte contains PEO and LiTFSI salt, with LAGP filler (1:1 weight ratio to PEO) and EMITFSI (0% − 40% weight ratio to PEO).

Results and Discussion

As both organic solid electrolyte (represented by PEO) and inorganic solid electrolyte (represented by LAGP) have their intrinsic inferiorities, these two types of electrolyte materials were combined for better ion conduction properties. The optimized LAGP to PEO ratio was firstly determined based on the ionic conductivity measurement. A series of EIS study for the PEO_{16}LiTFSI-LAGP (PL) composite electrolytes with varied LAGP content were performed as shown in Figure 1a. The ratio of ethoxy (EO) group to the Li^+ in LiTFSI salt was fixed at 16:1. As shown in the Figure S1(a-c) Nyquist plots, the high frequency intercept of the first semicircle at the real Z-axis represents the ohmic resistance of the LAGP phase (R_{LAGP}), while the lower frequency intercept represents an equivalent parallel resistance attributed to the bulk PEO (R_{PE}) and PEO-LAGP grain boundary (R_{GB}) conduction[30,31] represented by the equivalent circuit in Figure S1d. Since R_{PE} and R_{GB} cannot be individually separated from the Nyquist plot, herein the parallel resistors will be referred to as $R_{PE/GB}$ where $1/R_{PE/GB} = 1/R_{PE} + 1/R_{GB}$. An incomplete semicircle can be observed in the mid-frequency range at high LAGP loading, representing interfacial resistance (R_{INT}) against the blocking electrode, which diminishes with decreasing LAGP content and increasing temperature. The LAGP conduction measured from LAGP:PEO weight ratio ranging from 0.5 to 9 is shown in Figure 1a, while the conduction in the PEO and GB peaks at 1 before plummeting. This variation of conductivity can be attributed to the transition of the dominant Li transfer pathways as shown in Figure 1b.

For the PEO-LAGP composite electrolyte at low and intermediate LAGP loading (≤ 1), the LAGP particles act as plasticizer by locally disrupting the crystalline formation of PEO and provide additional Li^+ pathways along the amorphous LAGP-PEO grain boundary, thus improving the PE/GB ion conduction. As LAGP ratio increases to 1, the LAGP conductivity reaches a local maximum due to the additional ionic pathways provided by the bulk LAGP phase. This local maximum ratio is dependant on the morphology and treatment of the ceramic electrolyte, with reports ranging from 10% − 52.5%.[32–37] As LAGP loading further increases to an intermediate-high ratio (1−3), both LAGP and the PE/GB conductivity begins to drop. Li^+ crossing the PEO-LAGP interface requires overcoming the energy barrier at the interface.[10,38] The number of interfacial barriers increases with LAGP and competes with the tortuous grain boundary conduction pathway.[20,39] At high LAGP ratio (>3), the increasingly tortuous grain boundary conduction becomes a major bottleneck in Li^+ conduction, forcing diffusion pathways to favor the LAGP phase, resulting in an increase in LAGP conduction. Also, as shown in Figure 1c, the interfacial resistance (R_{INT}) of such composite electrolyte will increase with LAGP loading due to the insufficient PEO to facilitate the ionic transfer between LAGP particles and electrode surface. Whereas at LAGP ratio of 1, R_{INT} decrease from 233 to almost indistinguishable 2 Ω cm^2 at 35 and 50°C respectively. As a result, the LAGP to PEO ratio of 1 was taken as the optimized value in this study after taking the conductivity and cost control into consideration, which enables a considerable ionic conductivity of 2.46×10^{-5} S cm^{-1} at 35°C.

Subsequently, well-selected ionic liquid, i.e., EMITFSI was introduced into the optimized PL electrolyte for the preparation of PLE composite electrolyte due to its high conductivity and low viscosity. Typically, the PLE electrolyte was obtained by casting a homogeneous slurry containing proportional PEO, LiTFSI, LAGP, and EMITFSI in acetonitrile solvent and followed by vacuum drying under room temperature for 24 hrs (see details in Experimental). The PEO and LiTFSI amounts were controlled at [EO]:[Li] = 16:1, while the LAGP to PEO ratio was fixed at 1 as determined above. The EMITFSI addition was also controlled as a weight ratio to PEO from 0 to 40%.

The obtained electrolyte membrane delivers strong structural integrity and good flexibility in comparison with LAGP pellet and PL electrolyte membrane as shown in Figures 2a–2c (insets). This solution-based preparation is facile and efficient, which is highly favorable for large-scale fabrication. The SEM images show the typical surface morphology of different electrolytes. Due to the rigid

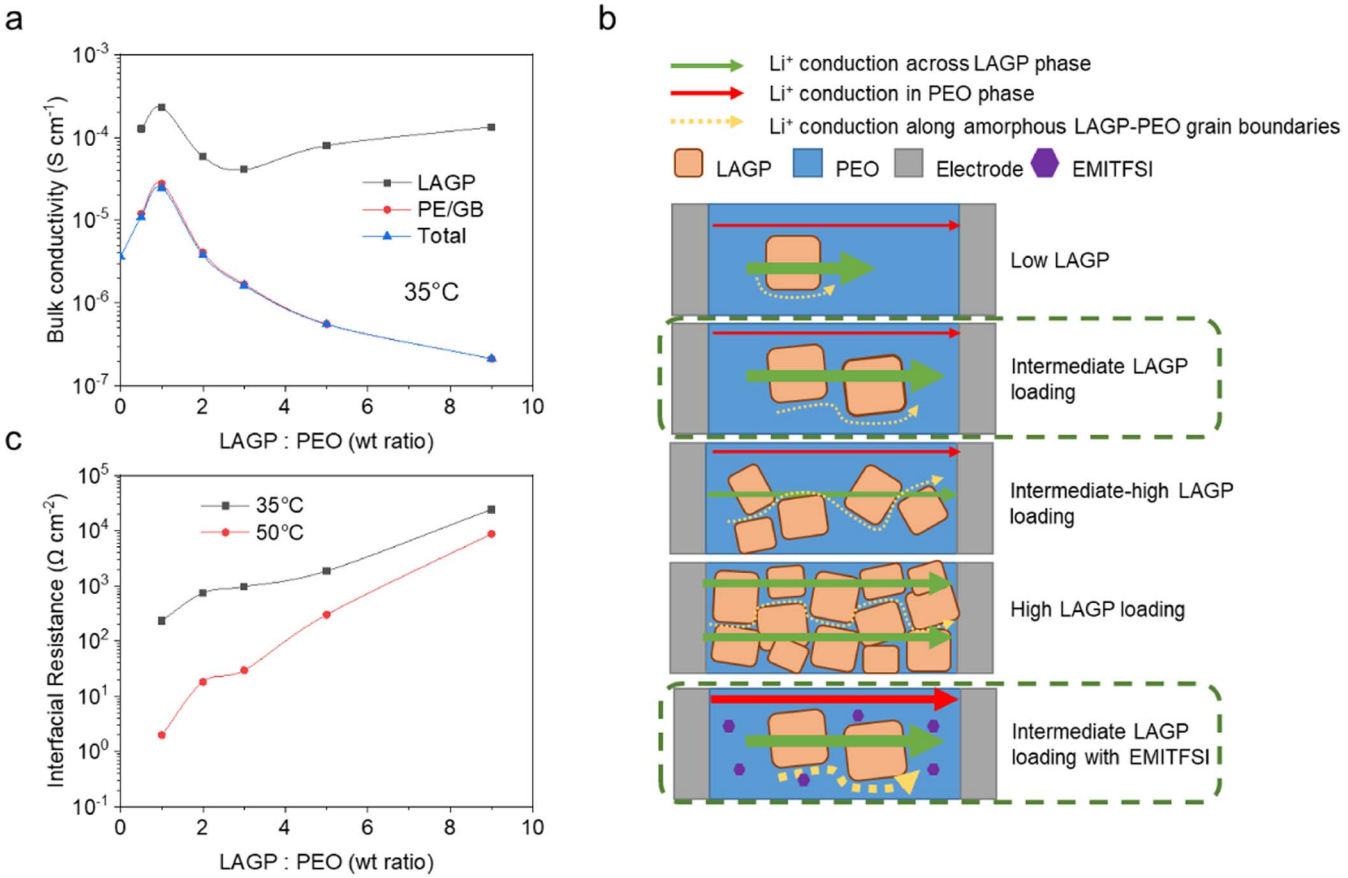

Figure 1. (a) Ionic conductivity of LAGP and bulk PEO & GB within the PEO_{16}LiTFSI-LAGP composite electrolyte with increasing LAGP to PEO ratios; (b) total bulk conductivity of composite electrolyte; (c) Schematic illustration of the transition of Li ion transfer pathway in PEO-LAGP composite electrolyte with different LAGP content.

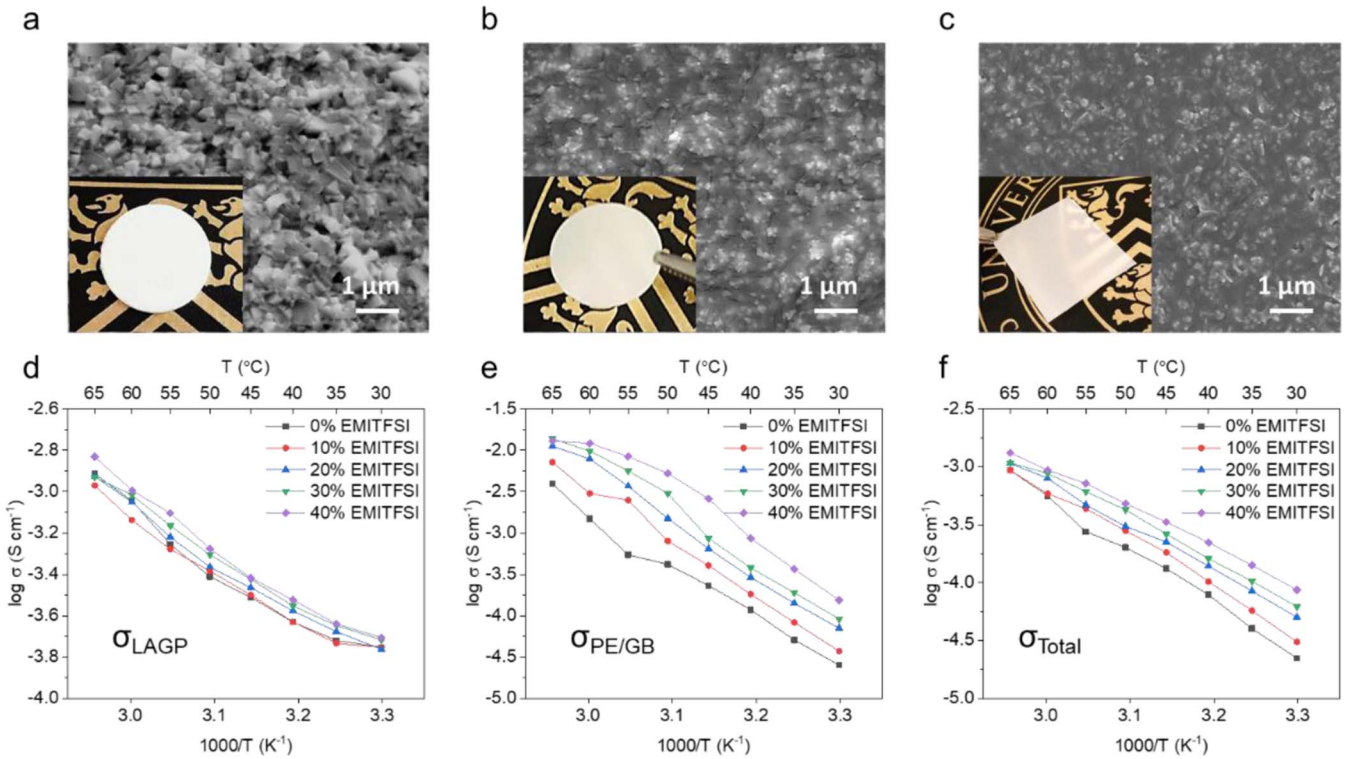

Figure 2. SEM and optical images (insets) of (a) LAGP pellet, (b) PL membrane and (c) PLE membrane; ionic conductivity attributed to (d) LAGP, (e) PEO/PEO-LAGP grain boundary, and (f) total bulk conductivity of PLE electrolyte with different of EMITFSI weight content at different temperature.

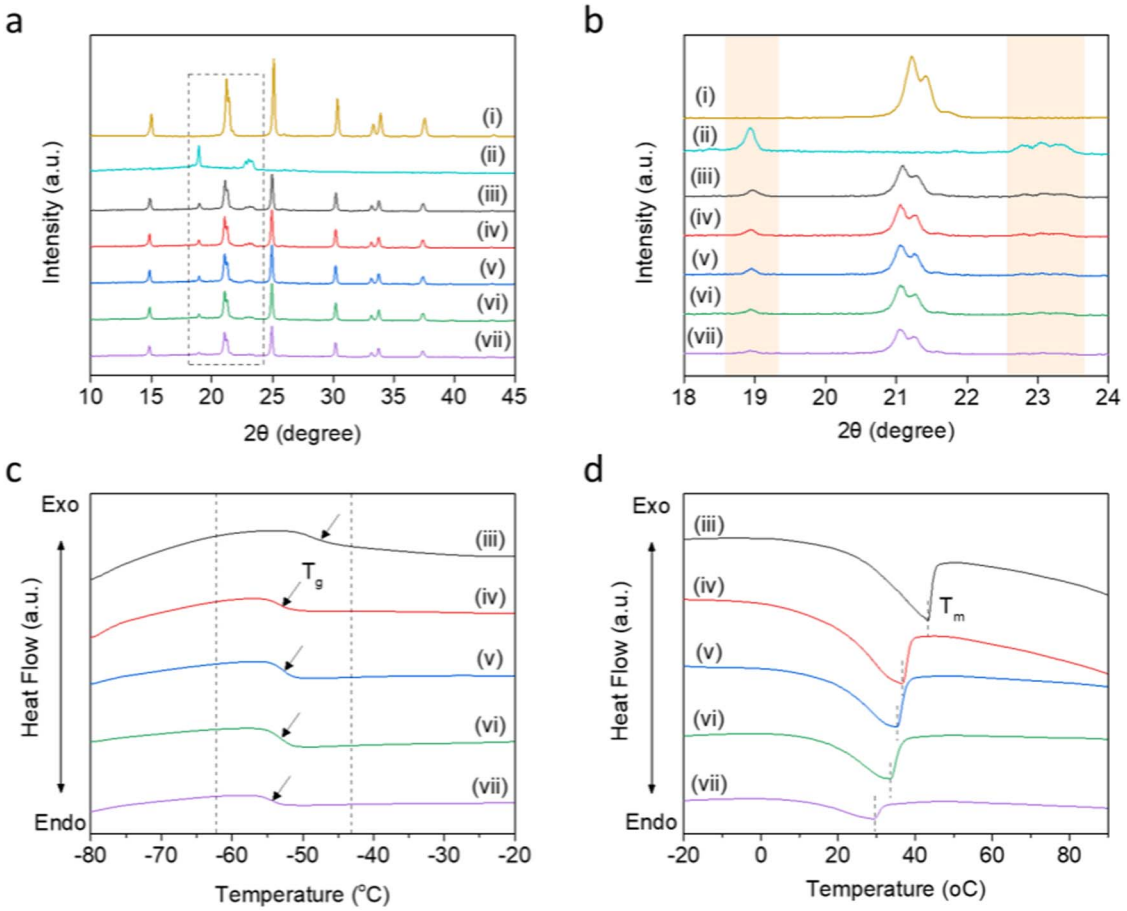

Figure 3. (a, b) XRD patterns and (c, d) DSC profiles of (i) LAGP powder, (ii) $PEO_{16}LiTFSI$, and (iii to vii) PLE electrolyte with 0, 10, 20, 30, 40% EMITFSI respectively.

powdery nature, the stacking of LAGP particles contributes to a rugged pellet surface, resulting in serious ion transfer barriers at the electrode/electrolyte interface and sluggish battery electrochemistry (Figure 2a). By contrast, the PL electrolyte membrane shows much smoother surface with LAGP homogeneously embedded within the PEO matrix (Figure 2b). The PEO segment well fills the interspaces, thus bridging the ion conduction between LAGP particles and enhancing the overall ionic conductivity. Meanwhile, the softer nature of PEO is expected capable of adapting to the electrode surface so as to improve the ionic contact at the electrode/electrolyte interface.[40–44] Notably, such favorable character was further strengthened by the introduction of EMITFSI in the composite as shown in Figure 2c. An intact and smooth surface with significantly less cracks can be observed for the obtained PLE composite electrolyte surface, which could further facilitate the interfacial ion transfer for a facile battery chemistry. The ion conductivities of the as-developed PLE composite electrolyte with different EMITFSI contents were investigated by EIS measurement (Figure S2). As shown in Figure 2d, conductivities attributed to LAGP follow a straight line with temperature in the Arrhenius plot with temperature having little effect, typical of a ceramic type solid electrolyte.[45,46] With addition of EMITFSI, σ_{LAGP} also increases slightly. This can be attributed to the plasticizing effect of EMITFSI which forms a better contact between PEO and LAGP particles, minimizing the PEO-LAGP interfacial resistance thus achieving a higher conductivity. Conductivity in the PEO/PEO-LAGP grain boundary phase ($\sigma_{PE/GB}$) is plotted in Figure 2e. Typical linear Arrhenius behavior is observed at high temperatures region, following a sudden increase in conductivity at the melting point. The jump in ionic conductivity is less obvious and also decreases with the increase of EMITFSI content due to the lower overall crystallinity.[47,42] Additionally, EMITFSI as a liquid does not suffer from aggregation issues as found in inert fillers such as SiO_2 and TiO_2 and meanwhile provides charge carriers EMI^+ and $TFSI^-$ for further improved ionic conductivity.[48,49] At 40% EMITFSI, $\sigma_{PE/GB}$ improvement tapers off at high temperature, which may be attributed to the promoted formation of Li^+-$TFSI^-$ ion pair that decreases ion mobility.[41] The total bulk conductivity is plotted in Figure 2f, where the lower temperature region conduction is limited by polymer phase conduction while at higher temperature, the conductivity of the LAGP phase becomes the limiting factor, resulting in an Arrhenius plot with mixed conduction mechanisms. The ionic conductivity of the PLE electrolyte continuously increases along with the augment of EMITFSI, while the decrease of interfacial resistance along with the increase of EMITFSI at different temperature can be perceived in Figure S3. At 40°C, PLE electrolytes containing EMITFSI no longer show any significant interfacial resistance. These results are consistent with the SEM observation that the introduction of EMITFSI favors interfacial contact and facilitates ion transfer. A high conductivity of 8.67×10^{-5} S cm^{-1} can be obtained for the PLE electrolyte with 40% EMITFSI at 30°C, which is much higher than that without EMITFSI (1.78×10^{-5} S cm^{-1}), indicating the significantly facilitated ion transfer by the introduction of ionic liquid.

In order to understand the underlying mechanism of this conductivity improvement, a series of XRD measurements were performed for different electrolytes as shown in Figure 3a. All the PLE composite electrolytes show sharp peaks in consistent with those in pure LAGP pattern, indicating that the LAGP well maintains its highly crystalline structure in the obtained composite. Moreover, the peaks at around

Table I. T_g, T_m, ΔH_m, and X_c of composite electrolytes obtained from DSC curves.

Ionic Liquid Content	T_g (°C)	T_m (°C)	ΔH_m (J g^{-1})	X_c (%)
0% EMITFSI	−49.3	43.2	90.8	42.5
10% EMITFSI	−54.3	36.5	80.8	37.8
20% EMITFSI	−53.5	35.2	71.4	33.4
30% EMITFSI	−53.2	33.5	58.0	27.2
40% EMITFSI	−54.3	29.2	26.4	12.4

19° and 23° are assigned to the crystalline phase of PEO.[50,49] It can be clearly observed in the enlarged area (Figure 3b) that the intensities of these peaks gradually decrease along with the increase of EMITFSI content in the composite, which indicates the continuous decrease of PEO crystallinity by the addition of EMITFSI.

This result can be further supported by the differential scanning calorimetry (DSC) analysis. The two endothermic transitions in Figure 3c and Figure 3d are assigned to the glass transition temperature (T_g) and melting temperature (T_m) of PEO respectively. The T_g, T_m, as well as the melting enthalpy (ΔH_m), and relative degree of crystallinity (X_c) values of different samples are summarized in Table I, where X_c is calculated based on the melting enthalpy of 100% crystalline PEO (203.0 J g^{-1}). The results clearly manifest the decrease for both T_m and T_g of the composite electrolyte by the introduction of EMITFSI, suggesting the essential role of EMITFSI as a plasticizer in PEO by weakening the interaction between PEO chains and partially preventing the recrystallization. The PEO crystallinity are strongly associated with the Li^+ conductivity in PEO matrix. The Li^+ conduction within PEO mainly relies on the intrachain and interchain hopping behaviors of Li^+ among the EO chains attributed to the high donor number of EO unit to Li^+.[51] Such mechanism is highly subject to the segment motion in polymer, where the higher chain flexibility contributes to faster ion transfer. Therefore, the higher amorphism of PEO allows for higher mobility of the EO chains and the resultant faster the Li^+ transfer within the PEO matrix.[52] Attributed to the decreased crystallinity, the transition of Li^+ conductivity from the low to high temperature region becomes smoother along with the increase of EMITFSI content as shown in Figure 2e. These results consistently confirm the lower PEO crystallinity and the resultant higher ionic conductivity by the introduction of EMITFSI in the composite electrolyte.

Apart from conductivity, the electrochemical stability and ionic transference number are also critical features for the feasibility and effectiveness of the as-developed composite electrolyte in solid state LIBs. Leaner Sweep Voltammetry (LSV) measurement was performed to investigate the electrochemical stability of different PLE electrolytes. As shown in Figure 4, PL composite without EMITFSI delivers anodic stability limit of around 4.5 V where oxidation of $TFSI^-$ is presumed to occur,[53] while its cathodic stability limit roughly 0 V. As EMITFSI is introduced into PL electrolyte, the cathodic stability limit was narrowed to around 1.5 V ascribed to the reduction of EMI^+ cation. Interestingly, the anodic limit of PLE electrolyte firstly expands to around 5.5 V and then decreases to around 4 V when a high EMITFSI content of 40% is added. The ability of EMITFSI to increase the anodic stability of PEO has been demonstrated.[54] The decrease at 40% EMITFSI is likely due to the increase in oxidation reaction of $TFSI^-$ overcoming such effect and thus lowering the anodic stability.[50,40] The overall stability windows for PLE electrolytes with less than 40% EMITFSI can reach around 4.0 V and cover the working voltage windows of most cathode materials. However, the relatively narrow stability limit of 40% EMITFSI sample may still cause unwanted decomposition of electrolyte during cycling and obstruct the electrochemical reversibility in the according cells.

Lithium transference number (t_{Li+}) was also evaluated for the as-developed PLE electrolyte. t_{Li+} is defined as the proportion of the electric current derived from lithium cations. Generally, non-aqueous liquid electrolytes have low t_{Li+} between 0.2 to 0.5 depending on the lithium salt,[55,56] which is similar to PEO-based solid polymer electrolytes with t_{Li+} typically lower than 0.5.[57,58] However, LAGP is a single-ion conductor allowing only Li^+ to conduct within and achieves t_{Li+} close to unity.[4] A high t_{Li+} indicates more current is carried by Li^+ than the $TFSI^-$ anions, and is favorable for high charge-discharge rates. Improved t_{Li+} can also decrease the Li^+ concentration gradient and discourage the growth of lithium dendrite by ensuring there's no depletion of Li^+ at the lithium anode surface at high current density.[59,60] The t_{Li+} of PLE electrolyte was measured via a combination of Chronoamperometry (CA) polarization and EIS techniques, and calculated based on Vincent-Evans equation from Eq. 1 (Figure S4). As shown in Table II, the composite electrolyte without EMITFSI has a high t_{Li+} of 0.88 attributed to the single-ion conducting nature of LAGP. The addition of 10% EMITFSI shows a decline of t_{Li+} to 0.77, followed by diminishing decline as further EMITFSI is added. Transference number for ionic liquid EMITFSI has been reported, with EMI^+ having higher mobility than $TFSI^-$, where t_{Li+} is 0.63,[61] hence agreeing with the experimental results. Consequently, although ionic conductivity increases with EMITFSI content, the contribution from anions also increases in proportion. The effective lithium ion conductivity (σ_{Li+}) is the product of σ_{total} and its respective t_{Li+}. It can be seen that σ_{Li+} still increases with increasing EMITFSI content despite the lowered t_{Li+}. However, it should be noted that the t_{Li+} of the PLE composite is still significantly higher than most PEO-salt solid polymer electrolyte, while the t_{Li+} decrease also becomes indistinctive since 20%. Therefore, taking the ion conductivity, electrochemical stability and

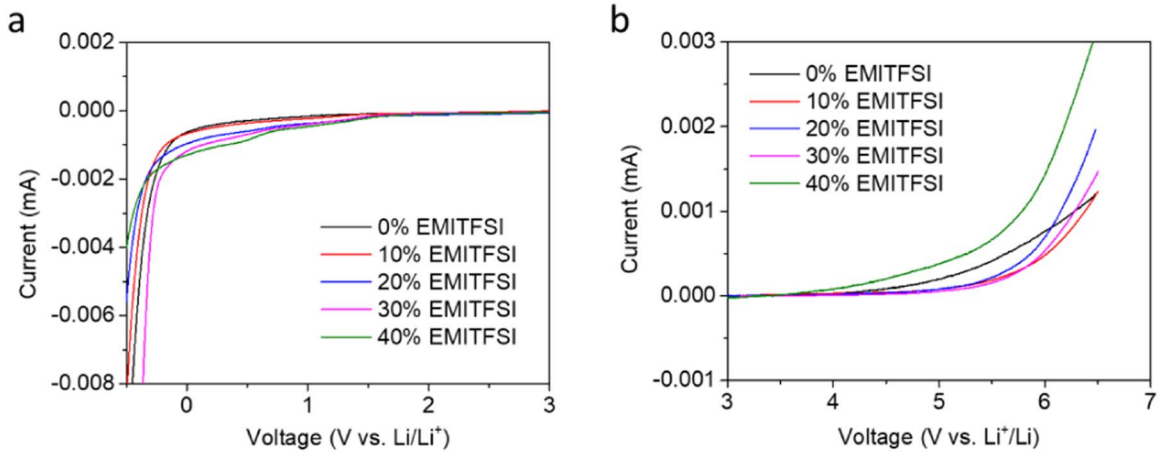

Figure 4. LSV curves of composite electrolyte with different EMITFSI content.

Table II. Calculation of t_{Li+} and σ_{Li+} utilizing Vincent-Evans equation performed at 50°C.

Sample	ΔV (V)	$R_{B,o}$ (Ω)	$R_{B,SS}$(Ω)	I_o (A)	I_{SS} (A)	t_{Li+}	σ_{Li+} (S cm^{-1})
0% EMITFSI	0.01	20.989	17.111	9.64×10^{-6}	8.56×10^{-6}	**0.88**	**2.01×10^{-4}**
10% EMITFSI	0.01	15.148	13.900	1.96×10^{-5}	1.53×10^{-5}	**0.77**	**2.81×10^{-4}**
20% EMITFSI	0.01	10.763	8.890	2.38×10^{-5}	1.76×10^{-5}	**0.73**	**3.07×10^{-4}**
30% EMITFSI	0.01	9.043	9.002	1.73×10^{-5}	1.25×10^{-5}	**0.72**	**4.26×10^{-4}**
40% EMITFSI	0.01	7.846	7.561	1.71×10^{-5}	1.24×10^{-5}	**0.72**	**4.82×10^{-4}**

lithium transference number into consideration, PLE electrolyte with 30% EMITFSI could be regarded as the optimized electrolyte composition, which may favor the better electrochemical performance of the according solid-state batteries.

The battery performance based on the as-developed PLE composite electrolyte was evaluated by using $LiFePO_4$ as cathode and lithium as anode in coin cell configuration. A high integration between cathode and electrolyte can be achieved benefiting from the solution-based fabrication (Figure S5a and b, fabrication details can be found in Experimental section). The cross-section SEM image in Figure S5c reveals the tight contact between cathode and electrolyte, which favors fast interfacial ion transfer and the resultant facile battery electrochemistry. Figure 5a shows the charge-discharge profiles of the $LiFePO_4$-Li cell at 0.3C based on PLE electrolyte with 30% EMITFSI. The voltage profile shows a typical discharge plateau at around 3.4 V and a charge plateau at around 3.5 V corresponding to the Fe^{3+}/Fe^{2+} redox, which is well consistent with literatures.[62–64] The relatively small potential gap between the charge and discharge plateaus indicates the fast redox kinetics attributed to the good ion conduction properties of the as-developed PLE electrolyte. In addition, the voltage profile well maintains during the cycling, indicating the good reversibility of the cell electrochemistry. The voltage profile of PLE samples containing differing amounts of EMITFSI can be seen in Figure S6. In line with the voltage profile, the CV curve shows a reduction peak at 3.12 V and oxidation peak at 3.61 V during the negative and positive scanning, respectively (Figure 5b). The peak position and intensity are also well maintained during the first several cycles, suggesting its good cycling stability. Figure S7 shows the EIS spectra of the obtained cell depicting typically a semicircle at high and medium frequencies and a slop at low frequency, which can be assigned the charge-transfer resistance (R_{ct}) and Warburg resistance respectively. Notably, the EIS results show significant resistance decrease along with the increase of EMITFSI due to its great improvement in ion conduction properties in the cells, which is consistent with the above results and signifies the expedited reaction kinetics, although cell with 40% EMITFSI exhibits a relatively larger resistance possibly

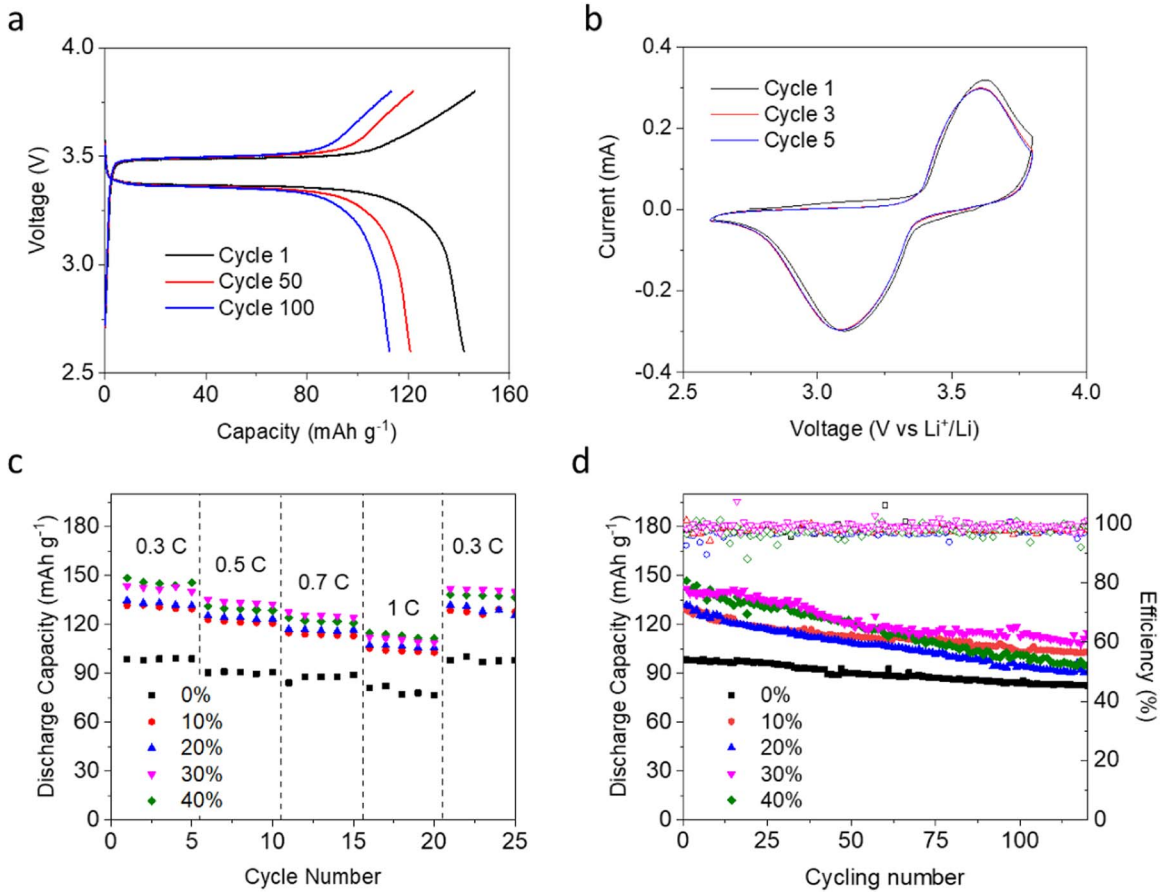

Figure 5. (a) Voltage profile and (b) CV curve of $LiFePO_4$-Li cell based on PLE electrolyte with 30% EMITFSI; (c) rate performance and (d) cycling performances at 0.3 C of $LiFePO_4$/PLE/Li cells based on PLE electrolyte with different EMITFSI content. The test temperature is 50°C.

ascribed to its inferior stability to Li metal. On this basis, multi-rate and galvanostatic cycling were performed for $LiFePO_4$-Li cells with different PLE electrolytes (Figures 5c and 5d). As expected, the participation of EMITFSI greatly enhances the reaction kinetics as the corresponding cells show much higher rate performance compared to that without EMITFSI. The cells with higher EMITFSI show better rate capability with 112.2 mAh g^{-1} for 30% and 114.7 mAh g^{-1} for 40% at raised current rate of 1C due to their higher ionic conductivity. Moreover, the cell based on PLE-30%EMITFSI electrolyte exhibits the best cycling stability with a high capacity retention of 114.7 mAh g^{-1} after 120 cycles, which is much higher than those with 0% (82.5 mAh g^{-1}), 10% (102.8 mAh g^{-1}), 20% (90.1 mAh g^{-1}), and 40% (94.6 mAh g^{-1}). Additionally, the coulombic efficiency well maintains at a relatively high level over 97%, elucidating its good electrochemical reversibility.

The increase in EMITFSI allows the electrolyte to attain higher ionic conductivity and better contact against the electrode, which facilitates an increased initial deliverable capacity. At a certain threshold, the overall benefit becomes overshadowed due to the instability of excess EMITFSI against lithium metal as shown in the LSV results. As EMITFSI content increases, the excess ionic liquid forms a more resistive SEI layer forms to pacify against the lithium electrode during cycling. Hence, despite PLE-40% EMITFSI exhibiting the highest conductivity, PLE-30% EMITFSI shows the most well balanced performance in terms of ionic conductivity, Li^+ transference number, and capacity retained at the end of the cycling period compared to other samples. These results demonstrate that good electrochemical lithium storage performance can be realized through the development and optimization of the IL-assisted organic-inorganic composite electrolyte as presented here, which shows good potential in promoting the solid electrolyte for the future energy storage application.

Conclusions

In the current work, we developed an IL-assisted organic-inorganic composite electrolyte for improved solid-state lithium-ion batteries. While taking advantage of the high conductivity and lithium transference number of LAGP, the EMITFSI serves as a plasticizer in the polymer phase of PEO-LAGP electrolyte, which effectively lowers the crystallinity of the composite and significantly enhances the overall ion conductivity. A high ionic conductivity of 4.26×10^{-4} S cm^{-1}, and decent Li^+ transference number of 0.72 were achieved at 50°C through the composition optimization. This further contributes to a good electrochemical performance of the $LiFePO_4$/PLE/Li cells, i.e., high cycling stability with 114.7 mAh g^{-1} after 120 cycles and decent rate capability of 112.2 mAh g^{-1} at 1C. The strategy developed in this work offers a new pathway toward low-cost and highly conductive electrolyte, which holds good promise in promoting the development of high-performance solid-state batteries for high-performance and safe energy storage.

Acknowledgment

This research was supported by the Natural Sciences and Engineering Research Council of Canada (NSERC) through grants to Z.C. and the University of Waterloo.

ORCID

Zhongwei Chen https://orcid.org/0000-0003-3463-5509

References

1. K. Funke, *Sci. Technol. Adv. Mater.*, **14**, 43502 (2013).
2. W. Li, Y. Pang, J. Liu, G. Liu, Y. Wang, and Y. Xia, *RSC Adv.*, **7**, 23494 (2017).
3. W. D. Richards, L. J. Miara, Y. Wang, J. C. Kim, and G. Ceder, *Chem. Mater.*, **28**, 266 (2016).
4. J. C. Bachman, S. Muy, A. Grimaud, H. H. Chang, N. Pour, S. F. Lux, O. Paschos, F. Maglia, S. Lupart, P. Lamp, L. Giordano, and Y. Shao-Horn, *Chem. Rev.*, **116**, 140 (2016).
5. Z. Huang, X. Yao, X. Xu, J. Yin, D. Liu, G. Peng, B. Huang, and C. Gao, *Chinese Phys. B*, **25**, 018802 (2016).
6. T. Liu, Y. Ren, Y. Shen, S. X. Zhao, Y. Lin, and C. W. Nan, *J. Power Sources*, **324**, 349 (2016).
7. R. Murugan, V. Thangadurai, and W. Weppner, *Angew. Chemie - Int. Ed.*, **46**, 7778 (2007).
8. B. Liu, Y. Gong, K. Fu, X. Han, Y. Yao, G. Pastel, C. Yang, H. Xie, E. D. Wachsman, and L. Hu, *ACS Appl. Mater. Interfaces*, **9**, 18809 (2017).
9. X. Han, Y. Gong, K. Kelvin Fu, X. He, G. T. Hitz, J. Dai, A. Pearse, B. Liu, H. Wang, G. Rubloff, Y. Mo, V. Thangadurai, E. D. Wachsman, and L. Hu, *Nat. Mater.*, **16**, 572 (2016).
10. W. E. Tenhaeff, K. A. Perry, and N. J. Dudney, *J. Electrochem. Soc.*, **159**, A2118 (2012).
11. T. R. Jow, J. L. Allen, J.-P. Jones, S. A. Delp, and M. C. Smart, *J. Electrochem. Soc.*, **165**, A361 (2018).
12. Z. Hu, Y. Chen, X. Hu, Y. Li, and Z. Ling, *J. Electrochem. Soc.*, **165**, A1269 (2018).
13. S. Ohta, Y. Kihira, and T. Asaoka, *Front. Energy Res.*, **4**, 1 (2016).
14. K. Nie, Y. Hong, J. Qiu, Q. Li, X. Yu, H. Li, and L. Chen, *Front. Chem.*, **6**, 1 (2018).
15. S. Chen, D. Xie, G. Liu, J. P. Mwizerwa, Q. Zhang, Y. Zhao, X. Xu, and X. Yao, *Energy Storage Mater.*, **14**, 58 (2018).
16. Z. Xue, D. He, and X. Xie, *J. Mater. Chem. A*, **3**, 19218 (2015).
17. D. Golodnitsky, E. Strauss, E. Peled, and S. Greenbaum, *J. Electrochem. Soc.*, **162**, A2551 (2015).
18. Y. Zhao, Z. Huang, S. Chen, B. Chen, J. Yang, Q. Zhang, F. Ding, Y. Chen, and X. Xu, *Solid State Ionics*, **295**, 65 (2016).
19. Q. Zhang, F. Ding, W. Sun, and L. Sang, *RSC Adv.*, **5**, 65395 (2015).
20. J. Zheng and Y. Hu, *ACS Appl. Mater. Interfaces*, **10**, 4113 (2018).
21. Y. Zhao, C. Wu, G. Peng, X. Chen, X. Yao, Y. Bai, F. Wu, S. Chen, and X. Xu, *J. Power Sources*, **301**, 47 (2016).
22. H. W. Kim, P. Manikandan, Y. J. Lim, J. H. Kim, S. C. Nam, and Y. Kim, *J. Mater. Chem. A*, **4**, 17025 (2016).
23. J. F. M. Oudenhoven, L. Baggetto, and P. H. L. Notten, *Adv. Energy Mater.*, **1**, 10 (2011).
24. Q. Guo, Y. Han, H. Wang, S. Xiong, Y. Li, S. Liu, and K. Xie, *ACS Appl. Mater. Interfaces*, **9**, 41837 (2017).
25. S.-M. Lee, Y.-C. Jung, D.-W. Kim, J.-H. Choi, and S. S. Jang, *J. Electrochem. Soc.*, **162**, A704 (2015).
26. C. Wang, Y. Yang, X. Liu, H. Zhong, H. Xu, Z. Xu, H. Shao, and F. Ding, *ACS Appl. Mater. Interfaces*, **9**, 13694 (2017).
27. K. M. Nairn, A. S. Best, P. J. Newman, D. R. MacFarlane, and M. Forsyth, *Solid State Ionics*, **121**, 115 (1999).
28. P. G. Bruce, J. Evans, and C. A. Vincent, *Solid State Ionics*, **28–30**, 918 (1988).
29. W. Liu, S. W. Lee, D. Lin, F. Shi, S. Wang, A. D. Sendek, and Y. Cui, *Nat. Energy*, **2**, 1 (2017).
30. D. Golodnitsky, A. Gladkich, D. Logvinuk, L. Burstein, R. Blanga, Y. Rosenberg, I. Shechtman, and M. Goor, *J. Solid State Electrochem.*, **20**, 3393 (2016).
31. S. Menkin, M. Lifshitz, A. Haimovich, M. Goor, R. Blanga, S. G. Greenbaum, A. Goldbourt, and D. Golodnitsky, *Electrochim. Acta*, **304**, 447 (2019).
32. Y. J. Wang, Y. Pan, and D. Kim, *J. Power Sources*, **159**, 690 (2006).
33. C.-W. Nan, J. B. Goodenough, L.-Z. Fan, Y. Li, L. Chen, and S.-P. Li, *Nano Energy*, **46**, 176 (2017).
34. J. Zhang, N. Zhao, M. Zhang, Y. Li, P. K. Chu, X. Guo, Z. Di, X. Wang, and H. Li, *Nano Energy*, **28**, 447 (2016).
35. S. Chen, Y. Zhao, J. Yang, L. Yao, and X. Xu, *Ionics (Kiel).*, **23**, 2603 (2017).
36. Q. Zhang, X.-B. Cheng, P.-Y. Chen, J.-Q. Huang, C.-Z. Zhao, X.-Q. Zhang, R. Xu, R. Zhang, and H.-J. Peng, *Proc. Natl. Acad. Sci.*, **114**, 11069 (2017).
37. S.-M. Lee, J.-H. Choi, C.-H. Lee, J.-H. Yu, and C.-H. Doh, *J. Power Sources*, **274**, 458 (2014).
38. F. La Mantia, M. S. Palagonia, R. Kun, F. Langer, I. Bardenhagen, and J. Glenneberg, *J. Electrochem. Soc.*, **164**, A2298 (2017).
39. J. Zheng, M. Tang, and Y. Y. Hu, *Angew. Chemie - Int. Ed.*, **55**, 12538 (2016).
40. P. Karner and Mandfred. Johansson, *Batteries*, **4**, 10 (2018).
41. H. Gupta, Shalu, L. Balo, V. K. Singh, S. K. Chaurasia, and R. K. Singh, *RSC Adv.*, **6**, 87878 (2016).
42. K. Kimura and Y. Tominaga, *J. Electrochem. Soc.*, **164**, A3357 (2017).
43. N. H. A. M. Hashim and R. H. Y. Subban, *AIP Conf. Proc.*, 2031, 020021 (2018).
44. A. Karmakar and A. Ghosh, *AIP Adv.*, **4**, 087112 (2014).
45. J. Li, K. Takahashi, O. Yamamoto, M. Zhang, N. Imanishi, Y. Takeda, B. Chi, and J. Pu, *J. Electrochem. Soc.*, **159**, A1114 (2012).
46. Z. Zhang, S. Chen, J. Yang, G. Liu, X. Yao, P. Cui, and X. Xu, *Electrochim. Acta*, **297**, 281 (2019).
47. S. B. Aziz, T. J. Woo, M. F. Z. Kadir, and H. M. Ahmed, *J. Sci. Adv. Mater. Devices*, **3**, 1 (2018).
48. C. H. Park, D. W. Kim, J. Prakash, and Y. K. Sun, *Solid State Ionics*, **159**, 111 (2003).
49. S. K. Chaurasia and A. Chandra, *Solid State Ionics*, **307**, 35 (2017).
50. K. Karuppasamy, H. W. Rhee, P. A. Reddy, D. Gupta, L. Mitu, A. R. Polu, and X. Sahaya Shajan, *J. Ind. Eng. Chem.*, **40**, 168 (2016).
51. C. S. Kim and S. M. Oh, *Electrochim. Acta*, **45**, 2101 (2000).
52. H. M. J. C. Pitawala, M. A. K. L. Dissanayake, V. A. Seneviratne, B. E. Mellander, and I. Albinson, *J. Solid State Electrochem.*, **12**, 783 (2008).
53. S. Kazemiabnavi, Z. Zhang, K. Thornton, and S. Banerjee, *J. Phys. Chem. B*, **120**, 5691 (2016).

54. C. Zhu, H. Cheng, and Y. Yang, *J. Electrochem. Soc.*, **155**, 569 (2008).
55. K. Xu, *Chem. Rev.*, **104**, 4303 (2004).
56. S. Zugmann, M. Fleischmann, M. Amereller, R. M. Gschwind, H. D. Wiemhöfer, and H. J. Gores, *Electrochim. Acta*, **56**, 3926 (2011).
57. J. Evans and C. Vincent, *Polym. (United Kingdom)*, **28**, 2324 (1987).
58. L. Niedzicki, M. Kasprzyk, K. Kuziak, G. Z. Żukowska, M. Armand, M. Bukowska, M. Marcinek, P. Szczeciński, and W. Wieczorek, *J. Power Sources*, **192**, 612 (2009).
59. C. Brissot, M. Rosso, J. N. Chazalviel, and S. Lascaud, *J. Power Sources*, **81**, 925 (1999).
60. K. M. Diederichsen, E. J. McShane, and B. D. McCloskey, *ACS Energy Lett.*, **2**, 2563 (2017).
61. M. Gouverneur, J. Kopp, L. Van Wüllen, and M. Schönhoff, *Phys. Chem. Chem. Phys.*, **17**, 30680 (2015).
62. A. A. Assegie, J. H. Cheng, L. M. Kuo, W. N. Su, and B. J. Hwang, *Nanoscale*, **10**, 6125 (2018).
63. A. Lassagne, E. Beaudoin, A. Ferrand, T. N. T. Phan, P. Davidson, C. Iojoiu, and R. Bouchet, *Electrochim. Acta*, **238**, 21 (2017).
64. G. B. Appetecchi, G. T. Kim, M. Montanino, F. Alessandrini, and S. Passerini, *J. Power Sources*, **196**, 6703 (2011).